Lecture 12: Organic templating of inorganic materials and bone biomimesis

---

Last time: interfacial biomineralization and biomimetic inorganic chemistry

Today: biological strategies for inorganic templating by organic materials
Biomimetic organic template materials
Biomimesis of bone

Reading: S. Mann, 'Biomineralization: Principles and Concepts of Bioinorganic Materials Chemistry,' Ch. 6, pp. 89-124 (2001)

Biological strategies for inorganic templating by organic materials

Alteration of barriers to nucleation

- Organic surfaces alter free energy barrier to nucleation (Mann Science 1993)

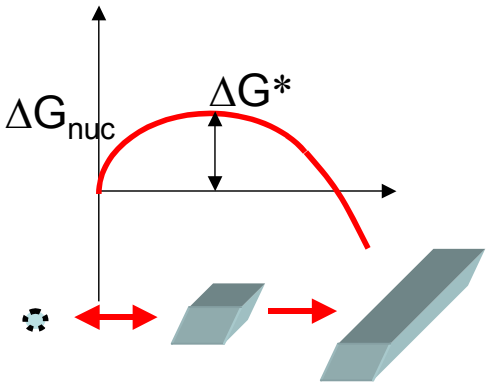

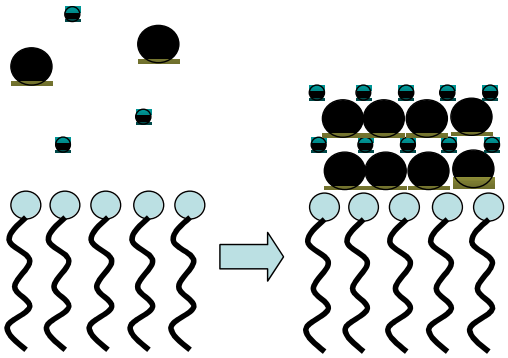

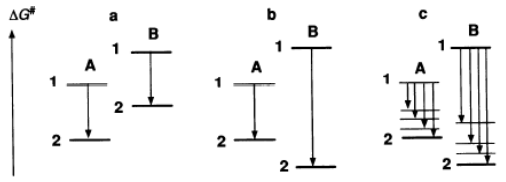

Fig. 2. Diagrammatic representation of the activation energies of nucleation, $\Delta G^{\#}$, of inorganic minerals in the absence (state 1) and presence (state 2) of an organic surface involved in biomineralization. Three possibilities exist for a mineral of two polymorphic structures (or two nucleation orientations), A and B, where A is the more kinetically favored in the absence of the organic matrix. (**a**) Nonspecific nucleation catalysis in which both polymorphs (or crystal faces) have reduced activation energies because of the presence of the matrix surface but there is no change in the outcome of mineralization. (**b**) Structure-specific nucleation of polymorph (or crystal face) B due to molecular recognition and high-fidelity synthesis or replication of the matrix surface. (**c**) Combination of (a) and (b) depending on the levels of recognition of nuclei A and B and the fidelity of matrix production, both of which may be influenced by genetic, metabolic, and environmental processes.

  - Reminder of free energy of nucleation (homogeneous, but principle applies to heterogeneous surface nucleation as well):

$$\Delta G_{nuc} = \Delta G_{surface} - \Delta G_{bulk} = 4\pi r^2\sigma - \frac{4}{3}\pi r^3 \frac{\Delta G_v}{V_m}$$

    - Where ΔGv is the free energy change for formation of the solid per mole from the ions, and Vm is the molar volume of the nucleated solid

- How are free energy barriers modified by organic templates? (Mann 1993) Complementarity in:

    1. Surface lattice geometries
    2. Spatial charge distributions
    3. Polarity of hydration layers
    4. Defect sites
    5. Bonding chemistry

        - Coordination environment of metal ion in crystal mimicked by binding to organic surface groups

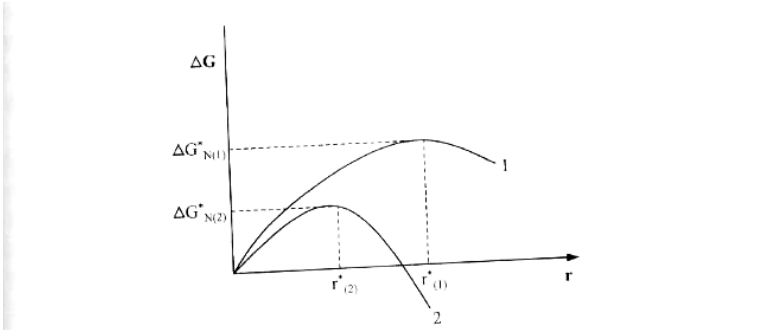

Fig. 6.28 Free energy curves for nucleation in the absence (1) and presence (2) of an organic surface.

- Matching lattice geometries:

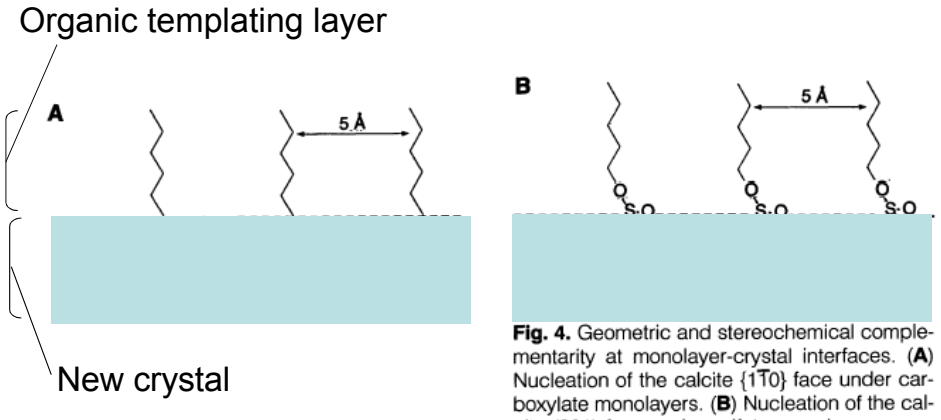

Fig. 4. Geometric and stereochemical complementarity at monolayer-crystal interfaces. (**A**) Nucleation of the calcite {1$\bar{1}$0} face under carboxylate monolayers. (**B**) Nucleation of the calcite (001) face under sulfate monolayers.

(Mann et al. 1993)

- Matching charge distributions:

    - Case of calcium cabonate: different crystal structures and crystal orientations nucleated on different charge surfaces

Table 1. Oriented nucleation of inorganic crystals under Langmuir monolayers.

System	Monolayer	[Metal] (mM)	Mineral	Nucleated face
$CaCO_3$	$CH_3(CH_2)_{16}COO^-$	7–10	Calcite	$\{1\bar{1}0\}$
		4–6	Vaterite	(001)
	$CH_3(CH_2)_{17}NH_3^+$	4–10	Vaterite	(001) + (110)
	$CH_3(CH_2)_{19}OSO_3^-$	10	Calcite	(001)
	$CH_3(CH_2)_{19}PO_3^{2-}$	10	Vaterite	(001)
	$CH_3(CH_2)_{17}OH$	4–10	Calcite + vaterite	Nonoriented + inhibited
	$C_{27}H_{45}OH$*	4–10	Calcite	Nonoriented
$BaSO_4$	$CH_3(CH_2)_{19}OSO_3^-$	0.15	Barytes	(100)
	$CH_3(CH_2)_{19}PO_3^{2-}$	0.15	Barytes	(100)
	$CH_3(CH_2)_{19}COO^-$	0.15	Barytes	(010)
$CaSO_4$	$CH_3(CH_2)_{17}NH_3^+$	20–40	Gypsum	(010) + $\{\bar{1}03\}$
	$CH_3(CH_2)_{19}OSO_3^-$	20–40	Gypsum	(010) + $\{\bar{1}03\}$
	$CH_3(CH_2)_{19}PO_3^{2-}$	20–40	Gypsum	(010) + $\{\bar{1}03\}$
	$CH_3(CH_2)_{19}COO^-$	20–40	Gypsum	(010) + $\{\bar{1}03\}$
	$CH_3(CH_2)_{17}OH$	20–40	Gypsum	(010)

*Cholesterol.

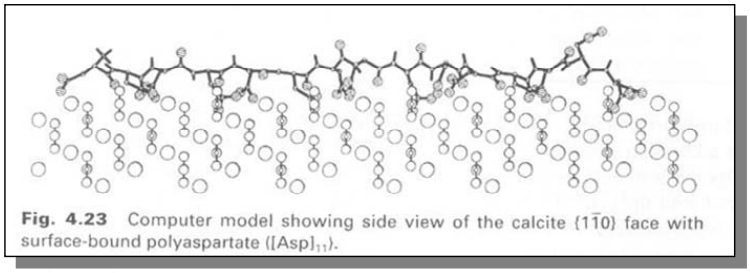

Fig. 4.23 Computer model showing side view of the calcite $\{1\bar{1}0\}$ face with surface-bound polyaspartate ($[Asp]_{11}$).

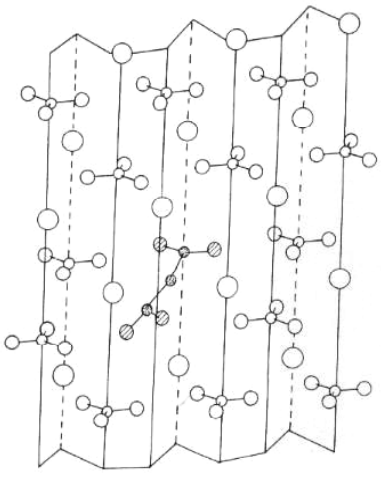

Fig. 4.20 Drawing of calcite $\{1\bar{1}0\}$ crystal face with surface-adsorbed malonate anion.

- Templates used by nature:
  - Proteins
  - Lipids
  - polysaccharides
- Process is universal for templated nucleation:
  - Material: carbonates, phosphates silica, ice
  - Template: carboxy-rich moieties hydrogen-bonding moieties
    - E.g. Aspartic acid, glutamic acid, phorphorylated residues for carboxy-rich
    - E.g. polysaccharides, Ser, Thr for hydrogen-bonding residues
  - (refs in Mann 1993)

control of nucleation and growth

- organic templates can preferentially nucleate the inorganic without ordering or aligning it
  - e.g. silica deposition in radiolarians and diatoms
- Templated crystal growth needs both recognition of individual molecules and a larger underlying lattice to drive directed nucleation
  - Obtaining periodicity in organic template:
    - How nature does it: secondary structures (nm-scale organization): α helix, β sheet
    - On larger length scales, cells control deposition
      - Localization and orientation of proteins and phospholipids
    - Secondary, tertiary, and quarternary protein structures are involved to provide the 'lattice' for templating crystals

- Ordered template geometries may allow selection of crystal polymorph
  - Requires flat, ordered surface in 2D
  - E.g. for $CaCO_3$: calcite vs. aragonite vs. vaterite

Calcium carbone ($CaCO_3$) crystal structures

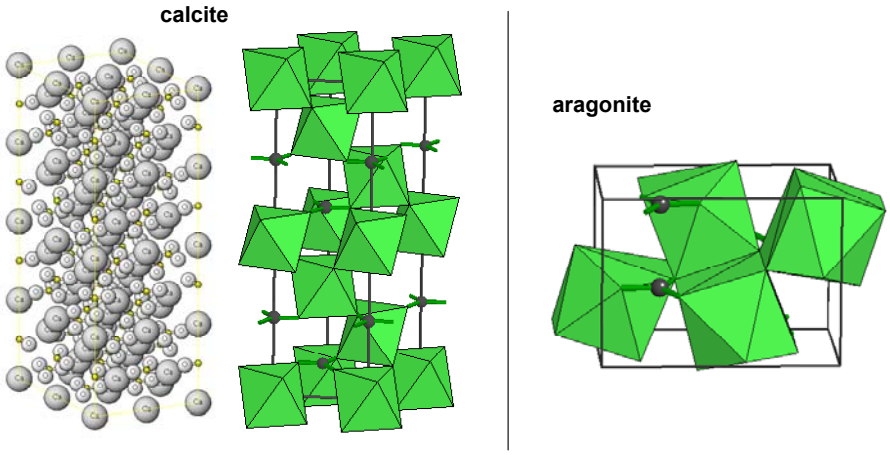

(http://ruby.coloarado.edu/~smyth/min/minerals.html)

- Example: nacre
  - Layered $CaCO_3$ structure of seashells (mollusks, etc.)

Plate-like aragonite ($CaCO_3$) crystals form the inner layer of seashells:

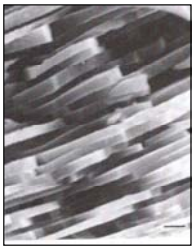

(scale bar 1 μm)

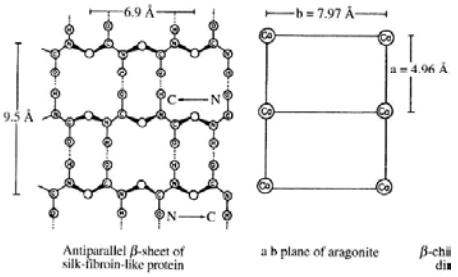

Fig. 6.38 Structural model for geometric matching in shell nacre.

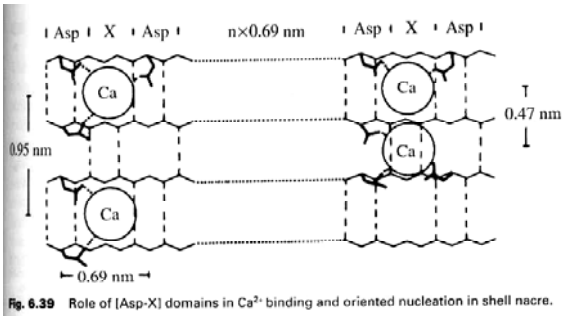

Fig. 6.39 Role of [Asp-X] domains in Ca^{2+} binding and oriented nucleation in shell nacre.

Biomimetic organic templated materials

Patterned surface mimics of templated inorganics[1]

Directed mineral deposition by patterned surfaces presenting organized charged groups[2,3]

- Work of Joanna Aizenberg at Bell Labs:

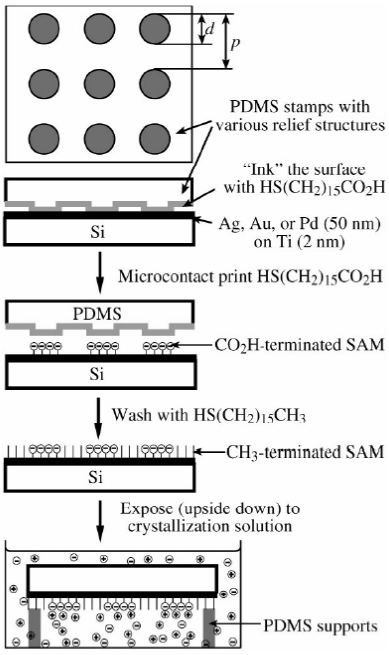

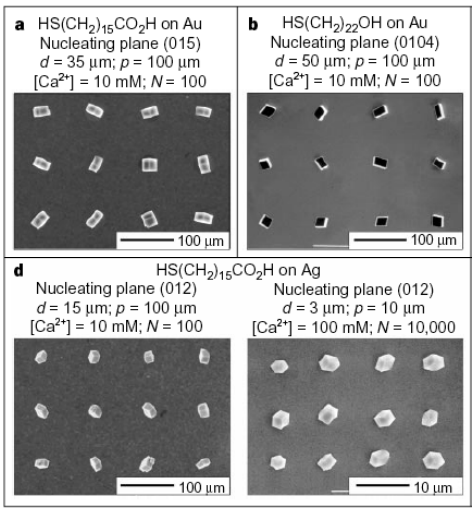

Figure 2 Ordered two-dimensional arrays of single calcite crystals. The densities of nucleation, uniform sizes and crystallographic orientation are controlled by the micropatterned SAMs consisting of regions of $HS(CH_2)_{15}X$ and $HS(CH_2)_{15}CH_3$. The density and sizes of features in the stamp and the concentration of the crystallizing solution were chosen to ensure the formation of one crystal per printed site. **a**, Arrays of crystals with the density of nucleation $N \approx 100$ crystals mm^{-2} grew selectively from the (015) plane on SAMs of $HS(CH_2)_{15}CO_2H$ supported on Au(111). **b**, Arrays of crystals with the density of nucleation $N \approx 100$ crystals mm^{-2} grew selectively from the (104) plane on SAMs of $HS(CH_2)_{22}OH$ supported on Au(111). **c**, Arrays of crystals with the density of nucleation $N \approx 1{,}000$ crystals mm^{-2} grew selectively from the (001) plane on SAMs of $HS(CH_2)_{11}SO_3H$ supported on Pd. **d**, Arrays of crystals nucleated selectively from the {012} plane on SAMs of $HS(CH_2)_{15}CO_2H$ supported on Ag(111) with various densities of nucleation: $N \approx 100$ crystals mm^{-2} (left) and $N \approx 10{,}000$ crystals mm^{-2} (right). **e**, An example of the fabrication of another complex crystalline pattern: a continuous, polycrystalline structure formed on SAMs consisting of a hexagonal array of 'stars' of $HS(CH_2)_{15}CH_3$ ($d = 12$ μm, $p = 15$ μm) in a field of $HS(CH_2)_{15}CO_2H$ on Ag(111). The low-magnification SEM (left) illustrates the high fidelity of the procedure, and the high-magnification fragment (right) shows the formation of uniform crystals of sub-micrometre sizes.

(Aizenberg et al. 2000)

- Supersaturation theory/model

crystal (crystals). The profiles were derived using the diffusior
$\partial c/\partial t = D\partial^2 c/\partial x^2$, and assuming zero concentration of solution at the
the crystallizing region (that is, assuming that all the ions that reach th
the crystal stick irreversibly). The dashed line corresponds to the conc
the saturated solution, c_{sat}, below which nucleation on the slowly
surface does not occur. In the region l_d where $c(x) < c_{sat}$, nucleation is
suppressed. Nucleation is allowed for distances from the rapidly
region, $x > l_d$, where $c > c_{sat}$. For the nucleation on the methyl-term
faces, c_{sat} is ~2.5 mM. **b**, SEM image of the pattern of calcite crystals
methyl-terminated surface with one isolated carboxylate-termina
showing the depletion distance, $l_d \approx 80\,\mu m$, in agreement with the v
100 μm) calculated assuming $c_{bulk} = 25$ mM, $c_{sat} = 2$–2.5 mM and cr
time $t = 30$ min. **c**, Calculated profiles of the concentration of the
solution in the vicinity of an array of rapidly nucleating regions with
$p < 2l_d$. The effective concentration (bold lines) over the entire slowly
region is then below c_{sat}. Crystallization will only take place on
nucleating regions, as shown in Fig. 1c.

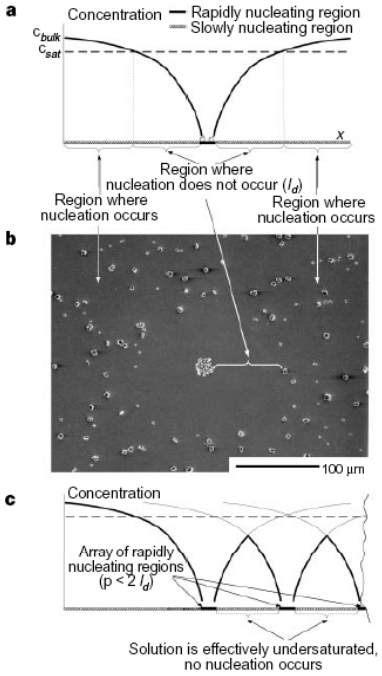

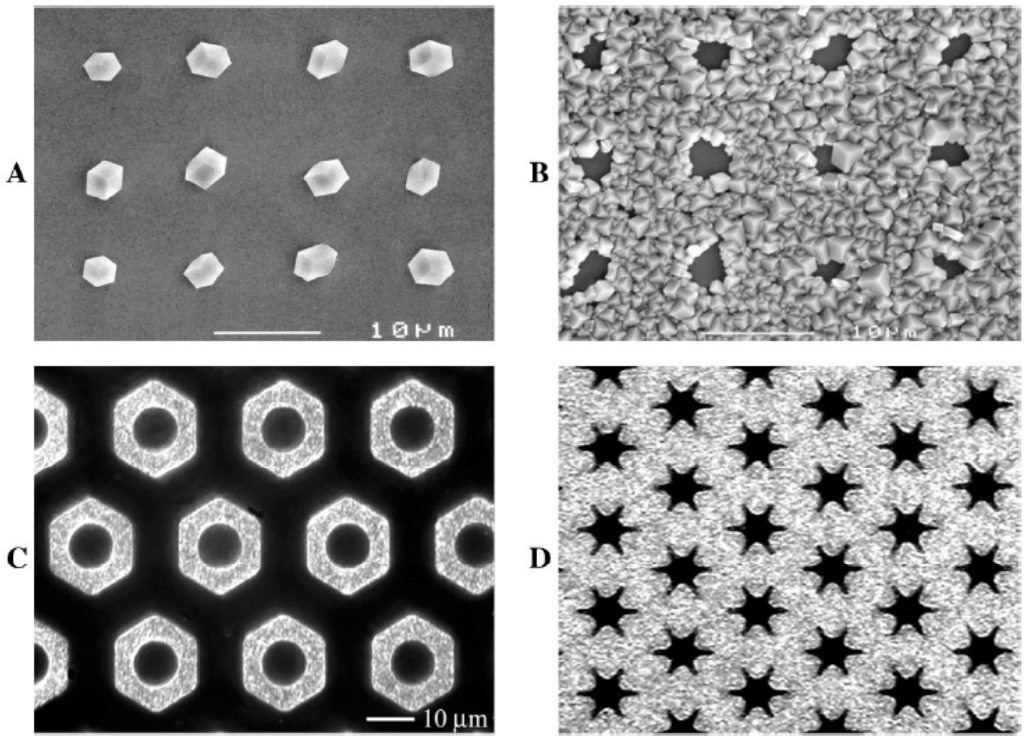

Mimicking the silica deposition of diatoms

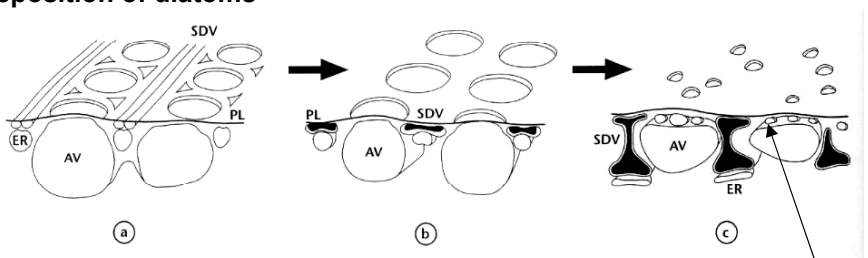

Fig. 7.15 Stages in the morphogenesis of the diatom frustule. See text for details.

nanovesicles

SDV - silica deposition vesicles
AV - aleolar vesicles
PL - plasmalemma (lipid bilayer cell wall)
ER - endoplasmic reticulum

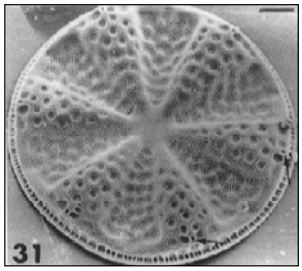

Disk-shaped diatom

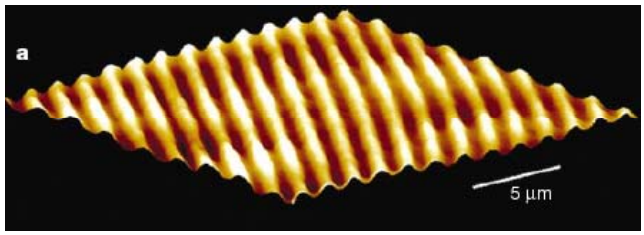

Silaffin cationic polypeptide lines SDVs and provides a nucleating surface for silica deposition in the diatom:

SSKKSGSYSGSGSKGSKRR

Amine side chains

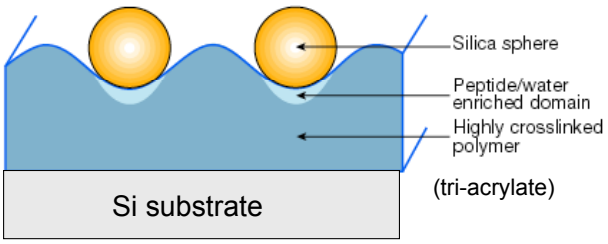

(Brott et al. 2001)

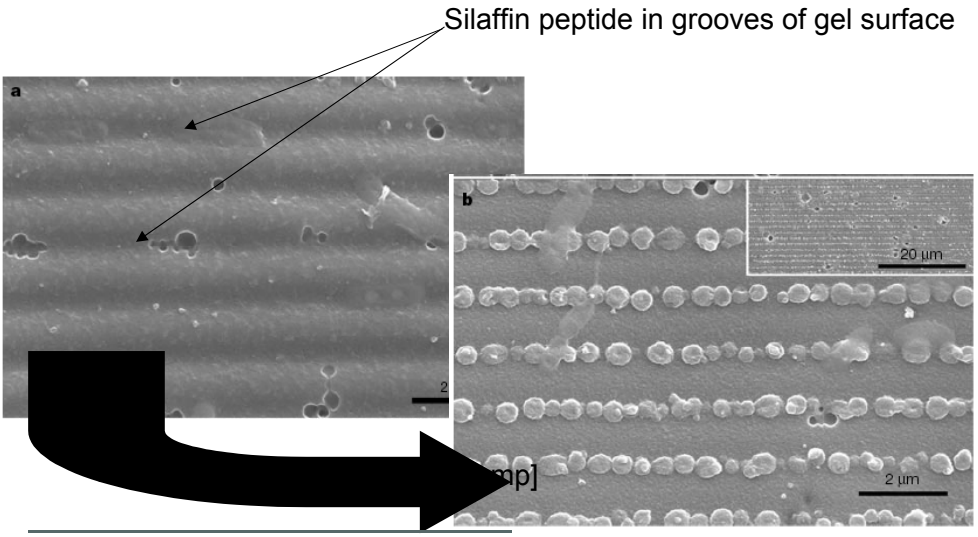

Reverse recognition: Using synthetic inorganic materials to guide localization of biological targets[4]

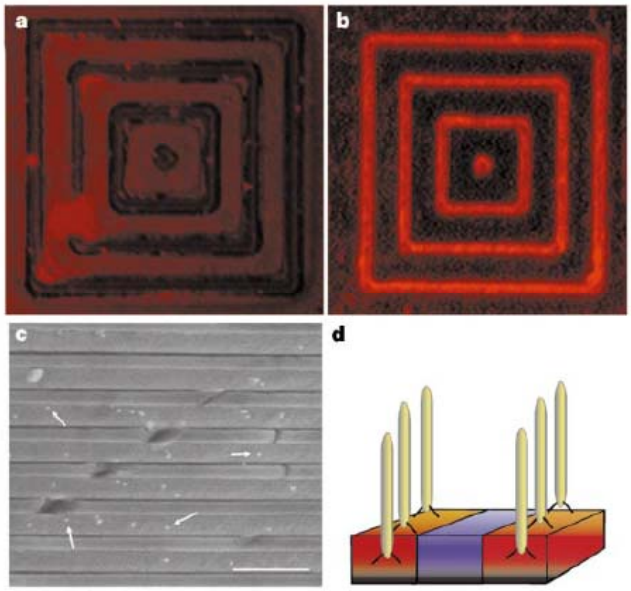

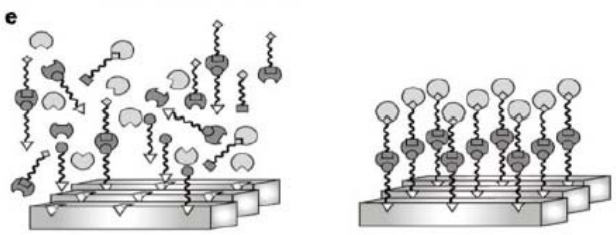

Figure 4 Phage recognition of semiconductor heterostructures. **a**–**c**, Fluorescence images related to GaAs recognition by phage. **a**, Control experiment: no phage is present, but primary antibody and streptavidin-tetramethyl rhodamine (TMR) are present. **b**, The GaAs clone G12-3 was interacted with a substrate patterned with 1-µm GaAs lines and 4-µm SiO_2 spaces. The phage were then fluorescently labelled with TMR. The G12-3 clone specifically recognized the GaAs and not the SiO_2 surface; scale bar, 4 µm. A diagram of this recognition process is shown in **d**, in which phage specifically attach to one semiconductor rather than another, in a heterostructure. **c**, An SEM image of a heterostructure containing alternating layers of GaAs and $Al_{0.98}Ga_{0.02}As$, used to demonstrate that this recognition is element-specific. The cleaved surface was interacted with G12-3 phage, and the phage was then tagged with 20-nm gold particles. These nanoparticles (shown arrowed in **c**) are located on GaAs and not AlGaAs layers. Scale bar, 500 nm. **e**, Diagram illustrating the use of this specificity to design nanoparticle heterostructures using proteins with multiple recognition sites.

(Belcher lab)

Biomimesis of bone

Structure of human bone

2 component model of organic matrix

- the organic matrix within bone is composed of 2 classes of organic materials

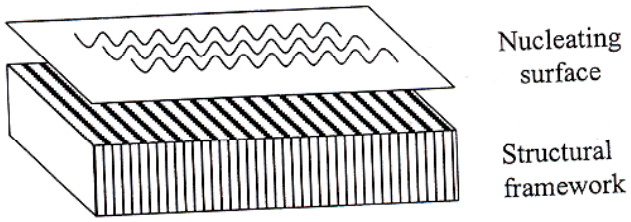

Fig. 6.4 Two-component model of the organic matrix.

  - crystals grown out from nucleating surface composed of acidic macromolecules

component	Composition	Water solubility	Role
Framework macromolecules	Hydrophobic/cross-linked proteins and polysaccharaides	Low	Matrix structural integrity
Acidic macromolecules	Glycoproteins and proteoglycans	High	Nucleating surface for hydroxyapatite

- components in human bones:

System	Framework macromolecules	Acidic macromolecules
Bone and dentine	Cross-linked type I collagen fibrils	Glycoproteins: Ostoepontin (these rich in Osteonectin Asp and Glu) Proteoglycans: Chondroitan sulfate Keratin sulfate
Tooth enamel	Amelogenin	Glycoproteins: enamelin

Organization of organic matrix

- framework macromolecules
  - tropocollagen cross-linked at helix ends in staggered arrangement
    - maximizes interfilament cross-links
  - each tropocollagen helix is 280 nm long
  - gaps between helices 40 nm x 5 nm '**hole zones'**

Human bone framework macromolecules:

Staggered arrangement of tropocollagen (triple helices) maximizes interfilament cross-links:

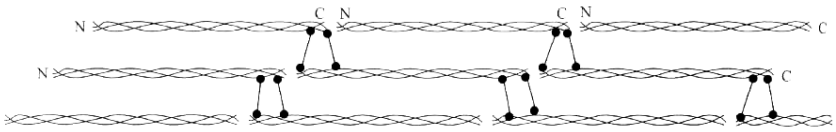

Fig. 6.11 Location of cross-links between the carboxy (C) and amino (N) terminal regions of adjacent tropocollagen filaments in collagen fibrils.

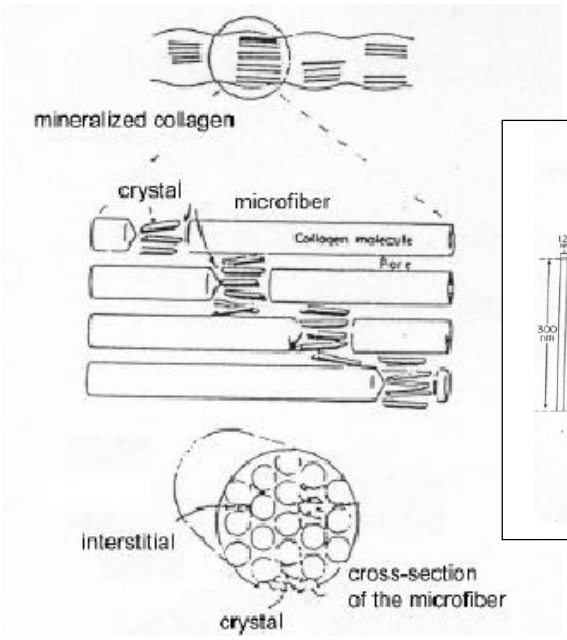

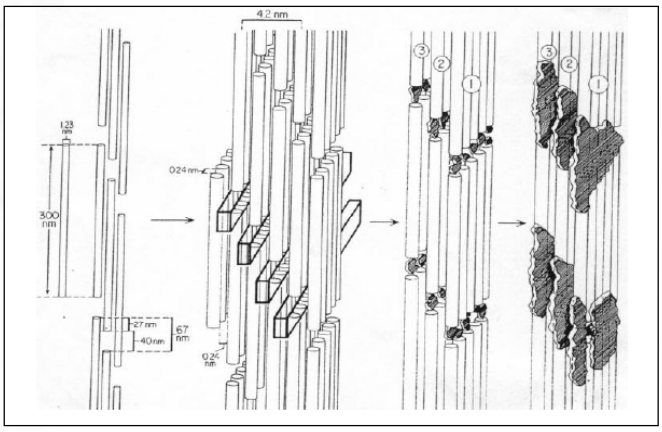

- glycoproteins bind collagen
  - exact role/organization is not yet known

- structural hierarchy
  - TEM micrograph in lamellar bone paper showing plywood structure[5]

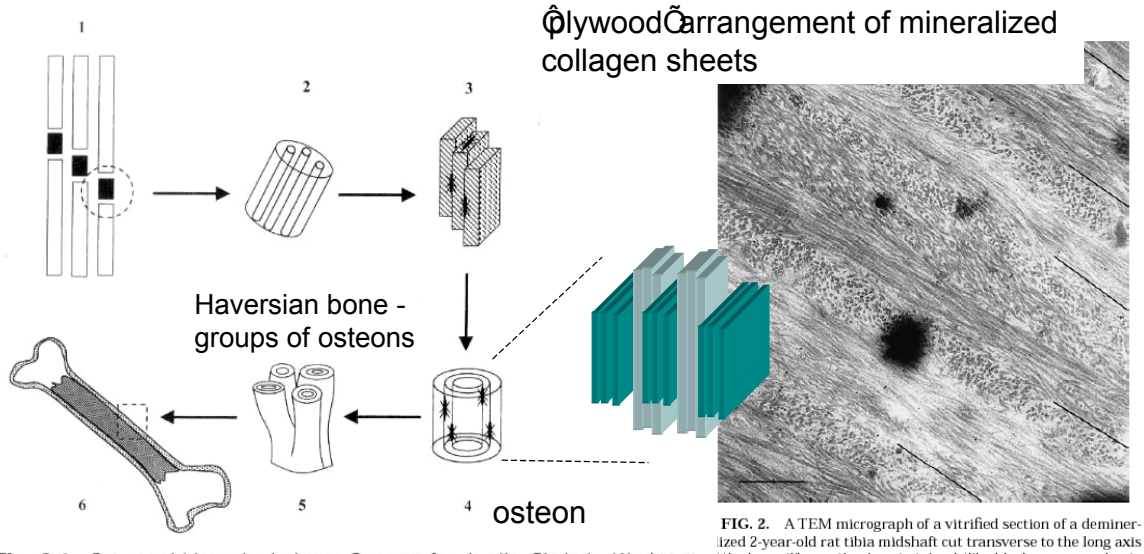

Fig. 8.1 Structural hierarchy in bone. See text for details. Circle in (1) shows the mineralization environment with hydroxyapatite crystal (black rectangle) within the hole zone of staggered tropocollagen molecules. Osteocytes are shown in (3) and (4) as black markings.

FIG. 2. A TEM micrograph of a vitrified section of a demineralized 2-year-old rat tibia midshaft cut transverse to the long axis of the bone. The section is not stained. The black areas are due to crystalline ice on the surface of the section. The sloping lines demarcate the boundaries between successive lamellar units, which are arbitrarily located adjacent to the sublayer with collagen fibrils in the plane of the section. The differing lengths of the sectioned fibrils reflect the angles at which they are aligned relative to the section surface. The sectioning itself probably introduces some disorder. Note too that the boundaries between lamellar units are not straight, but undulate. Scale bar, 1 μm.

- matrix assembly:

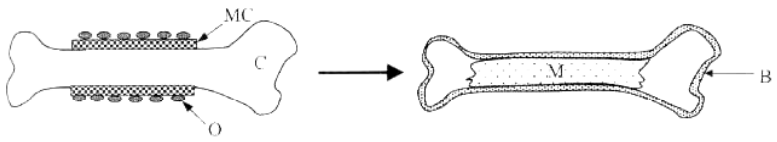

Fig. 8.2 Macroscopic shaping of long bones. C, cartilage preformer; O, osteoblasts; MC, mineralized collar; M, marrow; B, bone. See text for details.

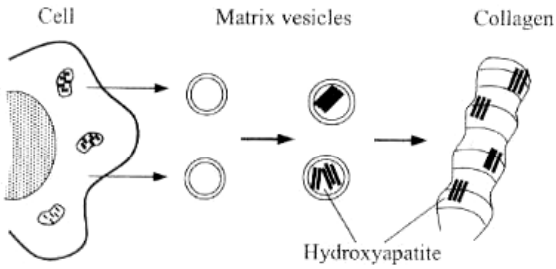

Fig. 8.3 Matrix vesicles in bone biomineralization.

(Mann, 2001)

synthetic attempts to mimic bone structure for biomaterials

- Stupp group at Northwestern University[6,7]
  - Mimicking hydroxyapatite localized growth using a self-assembling peptide amphiphile
  - SA peptide forms nanofibers – mimetic in mesoscale structure to collagen fibrils (though formed in a completely different way)

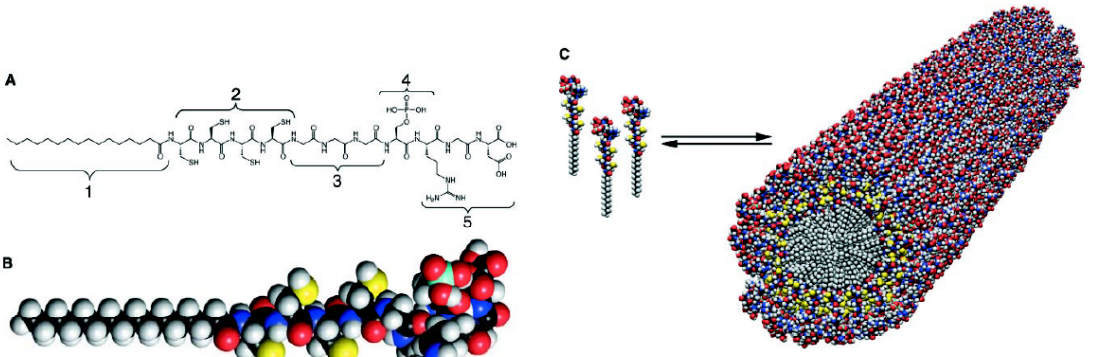

1. (**A**) Chemical structure of the peptide amphiphile, highlighting five key structural features. ɔn 1 is a long alkyl tail that conveys hydrophobic character to the molecule and, when ɔined with the peptide region, makes the molecule amphiphilic. Region 2 is composed of four consecutive cysteine residues that when oxidized may form disulfide bonds to polymerize the self-assembled structure. Region 3 is a flexible linker region of three glycine residues to provide the hydrophilic head group flexibility from the more rigid cross-linked region. Region 4 is a single phosphorylated serine residue that is designed to interact strongly with calcium ions and help direct mineralization of hydroxyapatite. Region 5 displays the cell adhesion ligand RGD. (**B**) Molecular model of the PA showing the overall conical shape of the molecule going from the narrow hydrophobic tail to the bulkier peptide region. Color scheme: C, black; H, white; O, red; N, blue; P, cyan; S, yellow. (**C**) Schematic showing the self-assembly of PA molecules into a cylindrical micelle.

(Hartgerink et al. 2001)

TEM of
Frozen fibers:

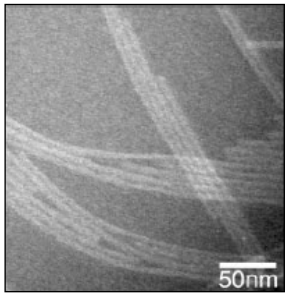

HA aligns with fibril axis

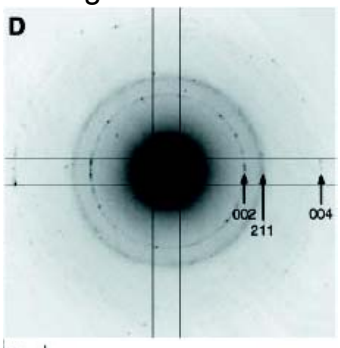

TEM of fibers incubated 30 min. in $CaCl_2/Na_2HPO_4$:

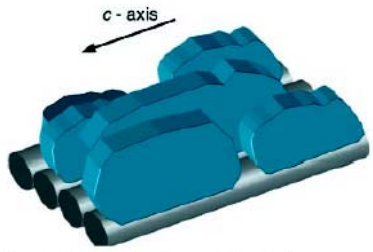

Fig. 4. Scheme showing relations between peptide-amphiphile fibers and hydroxyapatite crystals in the mineralized bundle. Arrow indicates the direction of the *c* axes of the crystals.

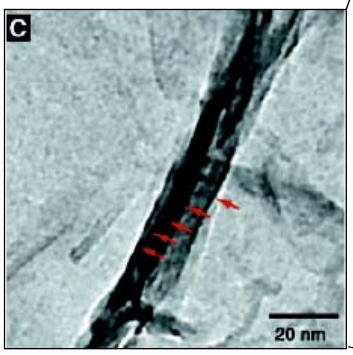

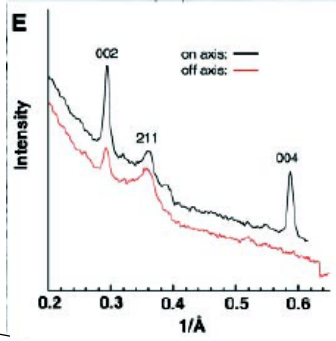

References

1. Brott, L. L. et al. Ultrafast holographic nanopatterning of biocatalytically formed silica. *Nature* **413**, 291-3 (2001).
2. Aizenberg, J., Black, A. J. & Whitesides, G. M. Control of crystal nucleation by patterned self-assembled monolayers. *Nature* **398**, 495-498 (1999).
3. Aizenberg, J. Patterned crystallization of calcite in vivo and in vitro. *Journal of Crystal Growth* **211**, 143-148 (2000).
4. Whaley, S. R., English, D. S., Hu, E. L., Barbara, P. F. & Belcher, A. M. Selection of peptides with semiconductor binding specificity for directed nanocrystal assembly. *Nature* **405**, 665-8 (2000).
5. Weiner, S., Traub, W. & Wagner, H. D. Lamellar bone: structure-function relations. *J Struct Biol* **126**, 241-55 (1999).
6. Hartgerink, J. D., Beniash, E. & Stupp, S. I. Peptide-amphiphile nanofibers: a versatile scaffold for the preparation of self-assembling materials. *Proc Natl Acad Sci U S A* **99**, 5133-8 (2002).
7. Hartgerink, J. D., Beniash, E. & Stupp, S. I. Self-assembly and mineralization of peptide-amphiphile nanofibers. *Science* **294**, 1684-8 (2001).